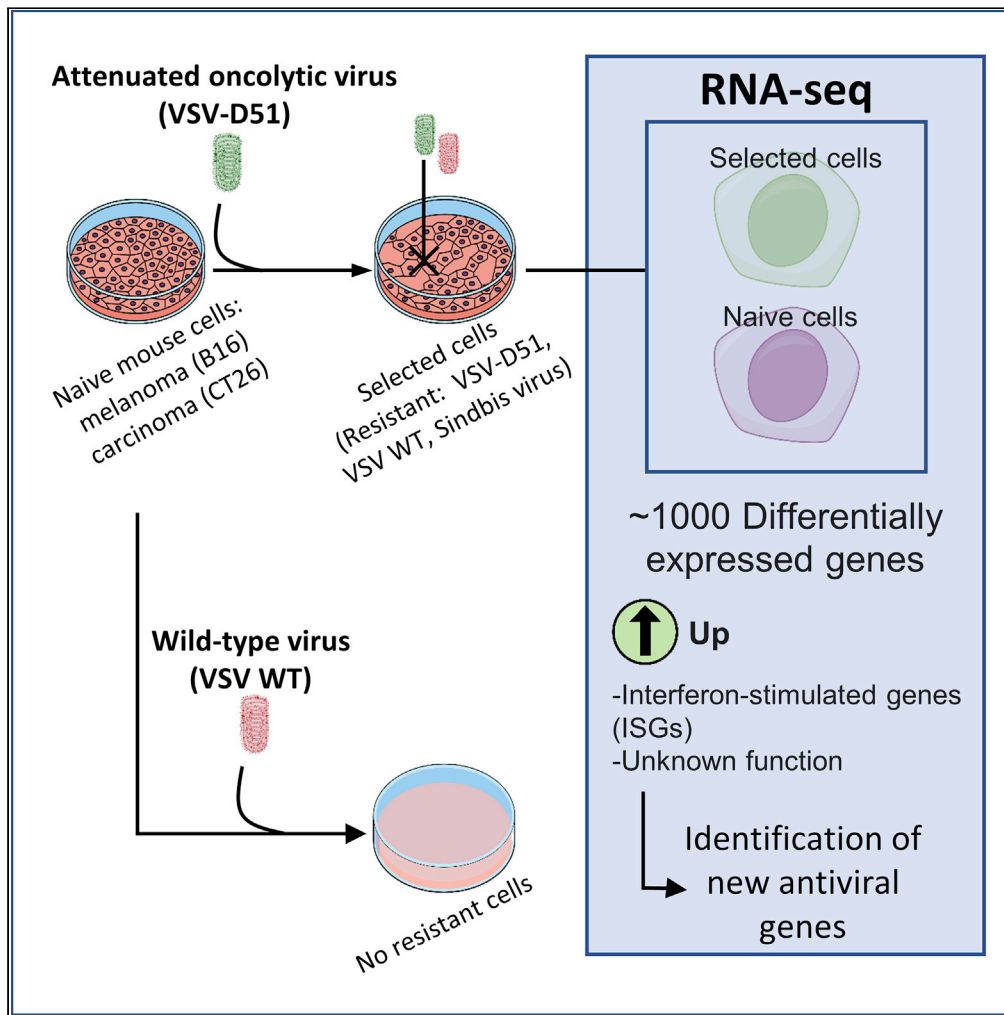


Article

Cellular resistance to an oncolytic virus is driven by chronic activation of innate immunity



Alejandra Larrieux, Rafael Sanjuán

rafael.sanjuan@uv.es

Highlights

Isolation of B16 VSV-resistant clones was associated to broad gene expression changes

Cytokine and innate immunity pathways mechanisms are involved in chronic VSV resistance

B16 and CT26 VSV-resistant clones showed correlated changes in gene expression patterns

In VSV-resistant clones, genes with undescribed antiviral function were dysregulated



Article

Cellular resistance to an oncolytic virus is driven by chronic activation of innate immunity

Alejandra Larrieux¹ and Rafael Sanjuán^{1,2,*}

SUMMARY

The emergence of cellular resistances to oncolytic viruses is an underexplored process that could compromise the efficacy of cancer virotherapy. Here, we isolated and characterized B16 mouse melanoma cells that evolved resistance to an oncolytic vesicular stomatitis virus (VSV-D51). RNA-seq revealed that resistance was associated to broad changes in gene expression, which typically involved chronic upregulation of interferon-stimulated genes. Innate immunity activation was maintained in the absence of the virus or other infection signals, and conferred cross-resistance to wild-type VSV and the unrelated Sindbis virus. Furthermore, we identified differentially expressed genes with no obvious role in antiviral immunity, such as *Mnda*, *Psmb8* and *Btn2a2*, suggesting novel functions for these genes. Transcriptomic changes associated to VSV resistance were similar among B16 clones and in some clones derived from the mouse colon carcinoma cell line CT26, suggesting that oncolytic virus resistance involves certain conserved mechanisms and is therefore a potentially predictable process.

INTRODUCTION

Oncolytic virotherapy offers an alternative treatment against several cancers.¹ Most tumor cells are more susceptible to viruses than healthy cells because augmented cellular proliferation often trades off with antiviral mechanisms.² Specifically, cancer cells usually show innate immunity defects, making them highly permissive to viruses.^{3,4} However, tumors exhibit micro-environmental and genetic diversity, which contributes to their survival under different types of stress, including anti-cancer treatments.⁵ Tumor adaptations include evasion or insensitivity to growth suppressor signals, inactivation of cell death mechanisms, resistance to hypoxia and chromatin remodeling, among others.^{6,7}

Previous work has investigated different virus resistance mechanisms.⁸ These include humoral and cellular antiviral adaptive immunity after multiple doses of a given virus,⁹ the activation of innate immunity pathways such as the interferon-receptor (IFNR)-based Janus-kinase (JAK-STAT) pathway,¹⁰ epigenetic modifications,^{11–13} hypoxia-driven inhibition of infection,¹⁴ APOBEC-mediated viral resistance,^{4,15} restrictions to viral binding and entry,¹⁶ autophagy,¹³ and tumor-associated spatial barriers.^{17–21} More specifically, the activation of master regulators such as the beta subunit of nuclear factor kappa-B kinase (IKK),²² as well as inositol polyphosphate 5-phosphatase (Inpp5e),²³ mitogen-activated protein kinase (MAPK),²⁴ multidrug-resistance protein-1 (MDR1),²⁵ mitogen-activated protein kinase kinase (MEK),²⁶ second mitochondria-derived activator of caspases (SMAC),^{27,28} sirtuin 1 (SIRT1),²⁹ and N-myc proto-oncogene protein (MYCN),³⁰ have been found to be associated with resistance to viral infection and replication in tumor cells.

Although changes in these features across tumor types are well-known to influence the success of oncolytic virotherapy, how naïve tumor cell populations respond to administration of an oncolytic virus is a largely unaddressed question. In principle, the selective pressure exerted by the virus in combination with tumor heterogeneity, should lead to the rapid selection of virus-resistant cells following treatment.³¹ Yet, it is currently unclear whether virus infection typically selects for changes in the expression of many genes or only a few. It is also unknown whether resistance mechanisms tend to be reproducible for a given cell type and virus or are highly variable and largely unpredictable.

Vesicular stomatitis virus (VSV) is one of the many viruses used for oncolytic virotherapy research and has been tested in several preclinical studies (e.g., NCT02923466 and NCT03865212). VSV presents a series of convenient features, including a relatively small, easy-to-manipulate genome, rapid replication, inability

¹Institute for Integrative Systems Biology (I2SysBio), Universitat de València-CSIC, Paterna, València 46980, Spain

²Lead contact

*Correspondence: rafael.sanju@uv.es

<https://doi.org/10.1016/j.isci.2022.105749>



to integrate into the host genome and lack of pre-existing immunity in humans.³² Moreover, VSV shows a remarkably wide cellular tropism, which in principle allows targeting multiple cancer types.³³ One of the best-studied oncolytic VSV is an engineered mutant carrying a deletion in methionine 51 of the matrix (M) protein (VSV-D51). This mutation suppresses the ability of the M protein to block nuclear RNAs export, allowing infected cells to mount antiviral immune responses.³⁴ As a result, VSV-D51 exhibits an attenuated phenotype in normal cells, but efficiently infects tumor cells that carry innate immunity defects.³⁵

In this study, we have explored the ability of cancer cells to evolve resistance against oncolytic viruses. To achieve this goal, we focused on VSV-D51 and mouse melanoma cells B16-F10, a well-studied murine cancer model.³⁶ We found that resistant cells readily emerged following infection with VSV-D51, and that these cells were not only resistant to VSV-D51, but also to wild-type VSV and the unrelated Sindbis virus. Transcriptomic analysis revealed an extensive genetic plasticity, with approximately 1000 differentially expressed genes in resistant cells compared to treatment-naïve cells. Changes in the interferon (IFN) signaling cascade represented a major mode of resistance, consistent with previous work involving human and mouse cell lines.^{31,37,38} In addition, resistant cells exhibited a marked (>1000-fold) over-expression of other genes that have not been previously implicated in antiviral defense, such as *Mnda1*, *Apol9* and *Psmb*, among others. Overall, differential gene expression patterns were highly correlated between resistant cell clones, and more interestingly, with the expression profile of a resistant clone obtained by the same selection procedure in CT26 mouse carcinoma cells, suggesting that the mechanisms responsible for the emergence of resistance to oncolytic therapy are reproducible, facilitating resistance management.

RESULTS

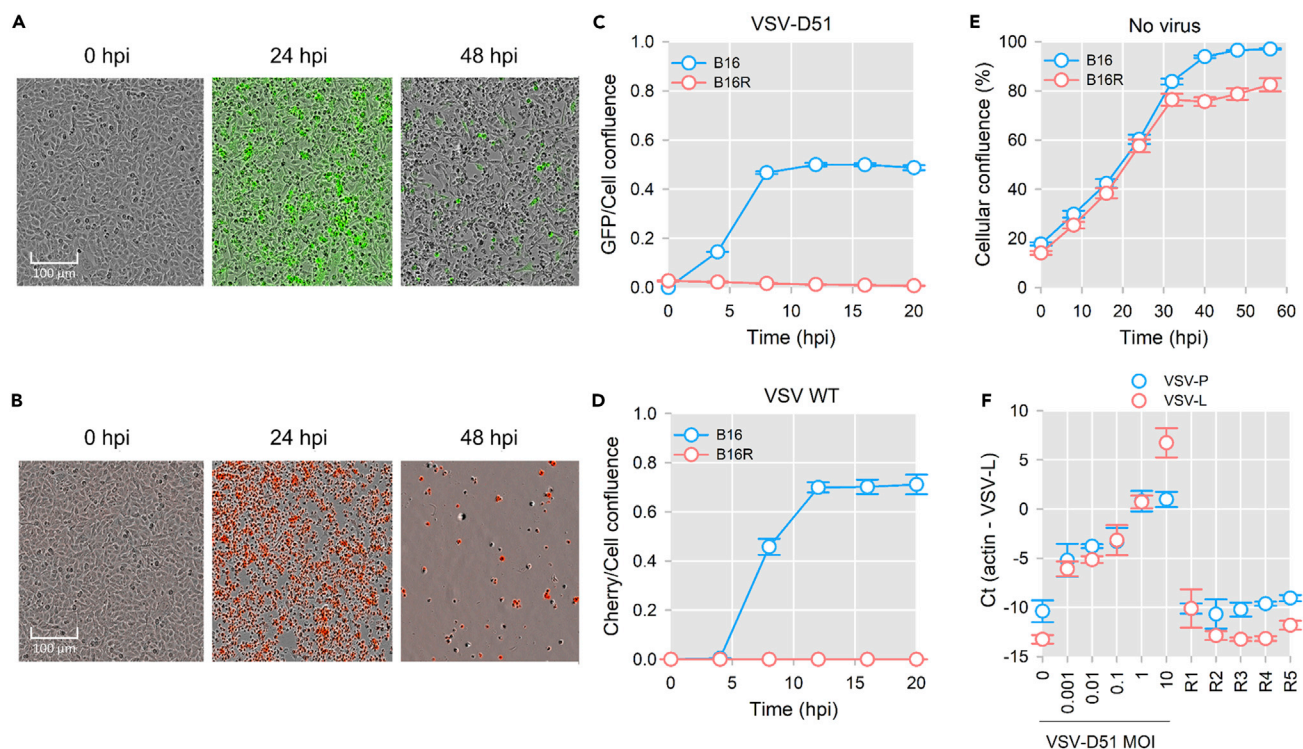
Isolation of VSV-resistant B16 cells

To select resistant B16 cells, we inoculated confluent cultures with a GFP-encoding VSV-D51 at a high multiplicity of infection (MOI = 5 plaque forming units, PFU per cell), washed out dead cells, allowed the culture to regrow for 72 h and iterated this process three times. We observed a high percentage of survivor cells despite the high MOI used (Figure 1A). We followed the same selection protocol using an mCherry-encoding wild-type (WT) VSV but, in contrast to the results obtained with VSV-D51, no surviving cells were recovered after multiple attempts (Figure 1B).

The selected cells became fully refractory to reinfection with VSV-D51, as determined by the lack of a detectable GFP signal following virus inoculation (Figure 1C). This suggests that the attenuated nature of VSV-D51 allowed some cells to respond to infection by undergoing changes that conferred antiviral resistance, or that cells became persistently infected with VSV-D51, making them insensitive to reinfection because of superinfection exclusion. Of interest, the recovered cells were refractory to infection not only with VSV-D51, but also with WT VSV (Figure 1D), revealing the involvement of mechanisms that were not specific to the oncolytic variant. In the absence of virus re-inoculation, the selected cells showed slightly reduced growth than naïve B16 cells (Figure 1E), suggesting a cost associated to resistance or persistence of infection.

Because selected cells may be a heterogeneous population and may still carry virus, five individual clones (R1-R5) were isolated by cell sorting and expanded. To test whether these derived clones contained virus, we first visualized GFP expression. All clones were GFP-negative. In addition, plaque assays indicated that no infectious particles were shed into the supernatants of these cultures. Furthermore, we extracted total cellular RNA and performed RT-qPCR of the VSV genes *P* and *L*, which yielded no amplification signal above background level (Figure 1F). We thus conclude that the five derived clones no longer contained VSV.

We then inoculated the five selected clones and naïve B16 cells with VSV-D51 to assess resistance. We monitored viral spread by measuring GFP signal in cells inoculated at low MOI (0.1 = PFU/cell) over a 24 h period using real-time live-cell microscopy. Moreover, supernatants were collected at endpoint (24 h after infection, hpi) and titrated to quantify viral progeny production. In addition, we used RT-qPCR to quantify viral RNA production (VSV-L) at 8 hpi. We found that R1, R2 and R5 exhibited a marked resistance to VSV-D51 infection by each of these three criteria (Figures 2A–2C; t-tests: $p < 0.001$), because GFP signal was below detection limit, viral titer at endpoint dropped between two and four orders of magnitude, and VSV-L RNA levels dropped between fourfold and >100 fold. In contrast, R3 and R4 showed only partial resistance, because GFP signal dropped less than twofold, whereas titers and RNA quantitation



showed no significant differences compared to naïve B16 cells. Overall, we found good agreement between GFP signal, titers, and RNA concentration, except for R2 cells, which showed orders of magnitude lower GFP and titer values, but experienced only a fourfold reduction in VSV-L RNA. This discrepancy might indicate that for this clone the resistance became effective in later stages of infection (translation, budding) or that it was dependent on the input MOI. We again found that in the absence of virus the derived clones showed slightly reduced growth than naïve B16 cells (Figure 2D), confirming a cost associated to resistance. Finally, to further assess resistance, we again monitored viral spread in cells inoculated with the three most resistant clones (R1, R2 or R5) at a higher MOI of 5 PFU/cell. GFP levels confirmed resistance in all cases (Figure S1).

Infection of R1, R2 or R5 with WT VSV (MOI = 0.1 PFU/cell) reproduced the results obtained with VSV-D51, (Figures S2A and S2B) confirming that the resistance mechanisms were not specific to the oncolytic variant. To further assess the generality of resistance, we also performed infections with Sindbis virus, which was capable to infect the naïve B16 cells (MOI = 1 PFU/cell). We found that Sindbis virus was unable to infect clones R1 and R5, whereas R2 cultures were infected albeit at slightly lower levels than naïve cells (Figure S2C).

VSV resistance is not mediated by enhanced antiviral cytokine signaling

We set out to test whether resistance was mediated by intercellular cytokine signaling. For this, we first primed naïve B16 cells with conditioned medium obtained from a previous infection of this same cell line with VSV-D51 (filtering out viral particles), inoculated these primed cultures with VSV-D51 (MOI = 0.1 PFU/cell), and followed viral spread by measuring GFP signal using real-time live-cell microscopy

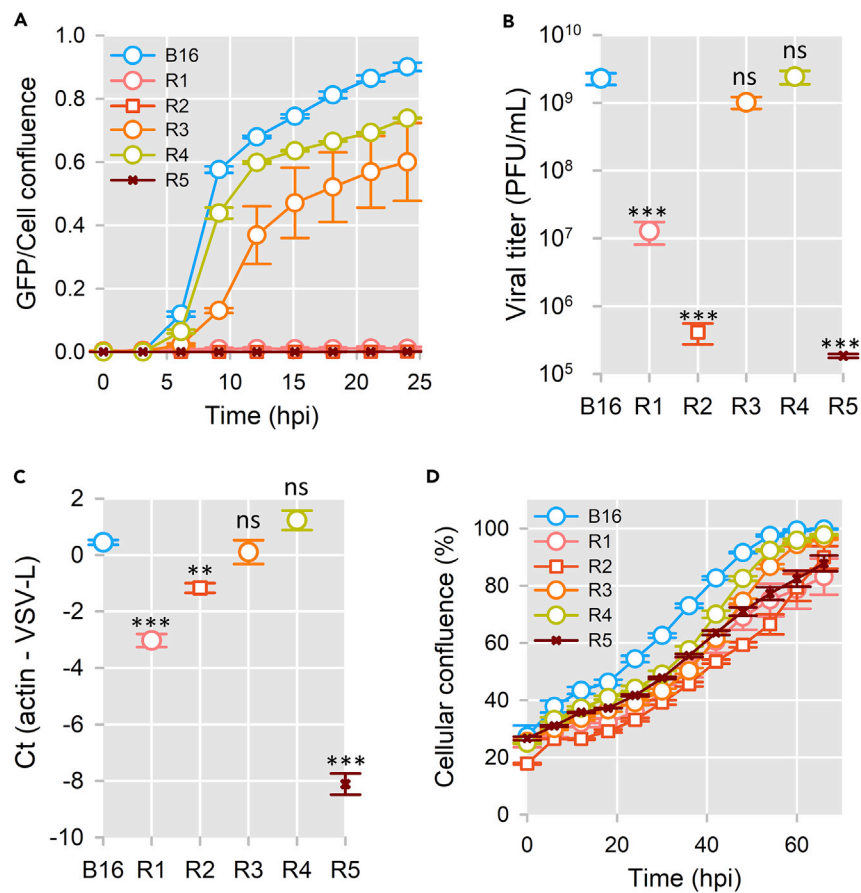


Figure 2. Analysis of VSV-resistant B16-derived clones

(A) Quantitation of infection by real-time live-cell fluorescence microscopy in naïve (B16) cells and derived clones R1-R5 inoculated with VSV-D51 (MOI = 0.1 PFU/cell).

(B) Titration of viral progeny produced at endpoint (24 hpi). Asterisks indicate significant differences with the naïve B16 cells by a t-test, using log-transformed data. *** $p < 0.001$; ** $p < 0.01$; ns: non-significant.

(C) RT-qPCR analysis of viral RNA produced in cells inoculated at low MOI (0.1 PFU/cell) after 8 hpi.

(D) Growth curves of B16 and B16R cell cultures in the absence of added virus. Data are presented as mean \pm SEM.

(Figure 3A). As expected, we found that B16 cells efficiently produced and responded to antiviral cytokines, as shown by the fact that infection progression was significantly reduced in the primed cultures. To examine antiviral cytokine production in the five resistant clones, we obtained conditioned media from R1-R5 infected cultures and used them to prime naïve B16 cells. Media obtained from the strongly resistant clones R1, R2 and R5 did not have an effect on infection spread. The simplest explanation for this observation is that, because the infection did not progress in these clones, there was little stimulus for cytokine production. The conditioned media collected from the partially resistant clones R3 and R4 did have an antiviral effect, but lower than that obtained from naïve B16 cells, probably for the same reason outlined for R1, R2 and R5.

Conversely, we obtained conditioned media from naïve B16 cultures infected with VSV-D51 and used it to prime R1-R5 cells (Figure 3B). R3 and R4 clones responded to this pre-treatment in a manner similar to normal B16 cells, whereas no infection signal was detected in primed cultures R1, R2, and R5 clones, as expected. We therefore obtained no evidence that VSV resistance was mediated by an increased production of or response to antiviral cytokines.

Transcriptomic analysis reveals chronic activation of antiviral innate immunity genes in VSV-resistant B16 cells

We used RNA-seq to study differences in the expression of genes that could be responsible for VSV resistance. For this, we focused on uninfected R1, R2, R5 clones and naïve B16 cells. For each, three independent RNA

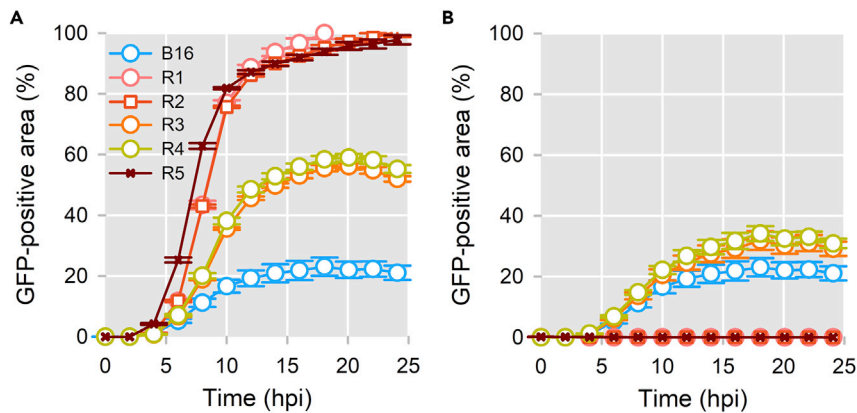


Figure 3. Conditioned media analysis for quantifying antiviral cytokine signaling

(A) Quantitation of infection by real-time live-cell fluorescence microscopy in naïve (B16) cell cultures, which were primed with virus-free media collected from a previous infection of the indicated cell line (B16, R1-R5), and then inoculated with VSV-D51 (MOI = 0.1 PFU/cell).

(B) Same analysis for B16 or R1-R5 cell cultures primed with virus-free media collected from a previous infection of naïve B16 cells, and then inoculated with VSV-D51 (MOI = 0.1 PFU/cell). Data are presented as mean \pm SEM.

extraction samples were sequenced. We obtained between 31.4 and 39.6 million clean reads per sample, with approximately 95% of the reads reaching a quality score of 30 or higher (Table S1). Paired-end reads were mapped to the *Mus musculus* genome. As expected, 90–94% of the mapped reads were in exons (Table S1). Approximately 84% of the genes were expressed at relatively low levels (FPKM <3), whereas <2% were strongly expressed (FPKM >60; Table S2). Pearson correlations between FPKM values obtained for the three RNA extractions of a given cell line were >0.99, indicating good reproducibility.

We analyzed differentially expressed genes by comparing normalized read counts in resistant clones versus naïve B16 cells. The number of genes exhibiting a statistically significant (adjusted $p < 0.05$) change in expression level of at least twofold was 928 for R1, 1025 for R2, and 1449 for R5, revealing broad differences between VSV-resistant clones and naïve cells (Figure 4A). Differential gene expression values (\log_2 fold change) were highly correlated between the three examined clones (R1 vs R2: Pearson $r = 0.848$; R1 vs R5: Pearson $r = 0.991$; R2 vs R5: Pearson $r = 0.845$ Figure 4B). Of the 50 top over-expressed genes in R1, 38 and 48 genes were also in the top-50 list for R2 and R5, respectively (Table S3). Similarly, of the 50 top under-expressed genes in R1, 12 and 35 genes were also in the top-50 list for R2 and R5 (Table S4). A principal component analysis revealed that the overall gene expression pattern of the three resistant clones clearly deviated from that of naïve cells and that, in turn, R1 and R5 showed similar gene expression patterns, which departed from that of R2 (Figure 4C).

An obvious pattern shared by all three resistant clones was the marked overexpression of antiviral innate immunity genes (Table S3). For instance, 2'-5'-oligoadenylate synthases (OAS) 1 and 2, which are central actors of the dsRNA-stimulated type-I IFN cascade³⁹ were overexpressed by >100-fold in each of the three resistant clones. Similar results were obtained for other IFN-stimulated genes (ISGs) such as Mx dynamin-like GTPase 2 (*Mx2*),⁴⁰ IFN regulatory factor 7 (*Irf7*),⁴¹ IFN-induced protein with tetratricopeptide repeats (*Ifts*),⁴² and apolipoprotein L9 (*ApoL9*).^{43–45}

A hierarchical clustering of gene expression profiles identified four gene clusters, of which two showed a clear overexpression in resistant clones compared to naïve cells (Figure S3). The first cluster (cluster A) consisted of 39 proteins which, according to a STRING analysis, tended to exhibit extensive functional interactions among them and were master regulators of innate immunity (*Irf7*, *Isg15*, *Usp18*, *Oasl1*, *Oasl2* and *Mx2* among others; Figure S4A). Some members of this cluster, such as myeloid cell nuclear differentiation antigen-like (*Mnda*), also showed a marked overexpression in resistant clones but did not appear to be connected to this interactome, despite the fact that *Mnda* has been recently shown to be an IFN-stimulated gene.^{46,47} The other cluster (cluster B) consisted of 113 proteins, of which four appeared within the top 50 most overexpressed genes in the three resistant clones (*Mnda*, *Csprs*, *Olfir56* and *Trim12a*). However, these proteins are not part of the complete interactome (Figure S4B).

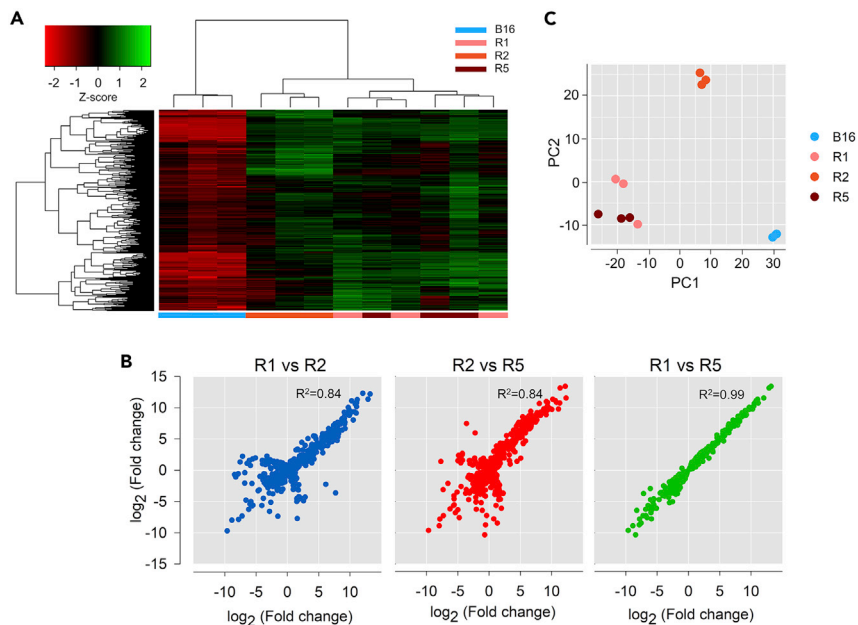


Figure 4. Differential gene expression analysis comparing resistant and naïve B16 cells

(A) Hierarchical clustering and heatmap showing differentially expressed genes between resistant (R1, R2, R5) and naïve B16 cells. The Z-score was calculated as $Z = (x - \mu) / \sigma$, where x represents the expression value of the gene in a given sample, μ the mean expression of that gene across samples, and σ the overall standard deviation. In the heatmap, red color indicates under-expressed genes and green color indicates over-expressed genes. The identity of each clone (naïve, R1, R2, R5) is indicated bottom bar associated legend.

(B) Correlation between differential gene expression data in the three isolated resistant clones.

(C) Principal component analysis of global gene expression in resistant and naïve B16 cells.

To obtain a more general overview of differentially expressed genes, we examined the Gene Ontology (GO) biological processes involved (Figure 5). For resistant clones R1 and R5, we confirmed a marked enrichment of pathways related to antiviral defense against viral infection. Processes related to immune response and response to viral infection were also significantly enriched in R2, although they were not among the most significantly enriched. In terms of the gene clusters identified above, the first cluster of 39 genes was clearly associated with innate immunity and antiviral defense, whereas the second cluster mainly showed an enrichment in pathways related to antigen presentation, negative regulation of viral release from the host cell, and negative regulation of viral replication.

Overall, these results show that the resistant clones experienced a sustained overexpression of antiviral genes in the absence of infection. GO terms also showed an increase in functions such as cell death induction and regulation of cellular response to stress, potentially explaining the lower proliferation rates of resistant clones compared to naïve cells. In contrast, the biological significance of downregulated genes was less clear. We found a >100-fold reduction in the expression levels of the butyrophilin subfamily 2 A2 (*Btn2a2*) gene, which is known to inhibit T cell-mediated immunity.⁴⁸ Glycosylase *Galnt6*, which has not been described to participate in antiviral immunity, was strongly repressed in clones R1 and R5, but not in R2.

Validation of RNA-seq results by qPCR and immunofluorescence

To verify the results obtained by RNA-seq, we measured the expression levels of *Mx2*, *Oasl* and *Irf7* by RT-qPCR in R1, R2, R5 and naïve B16 cells in the absence of virus. *Irf7* was undetected by this method in naïve B16 cells but was strongly expressed in R1 and R2, and clearly detected in R5 (Figure 6A). Moreover, the expression levels of *Mx2* and *Oasl* were orders of magnitude lower in naïve B16 cells than in the R1, R2, and R5 clones. To further validate these results, we performed *Mx2* immunoblotting in uninfected resistant and naïve cells. This confirmed *Mx2* expression in each of the three resistant clones, as opposed to naïve B16 cells (Figure 6B).

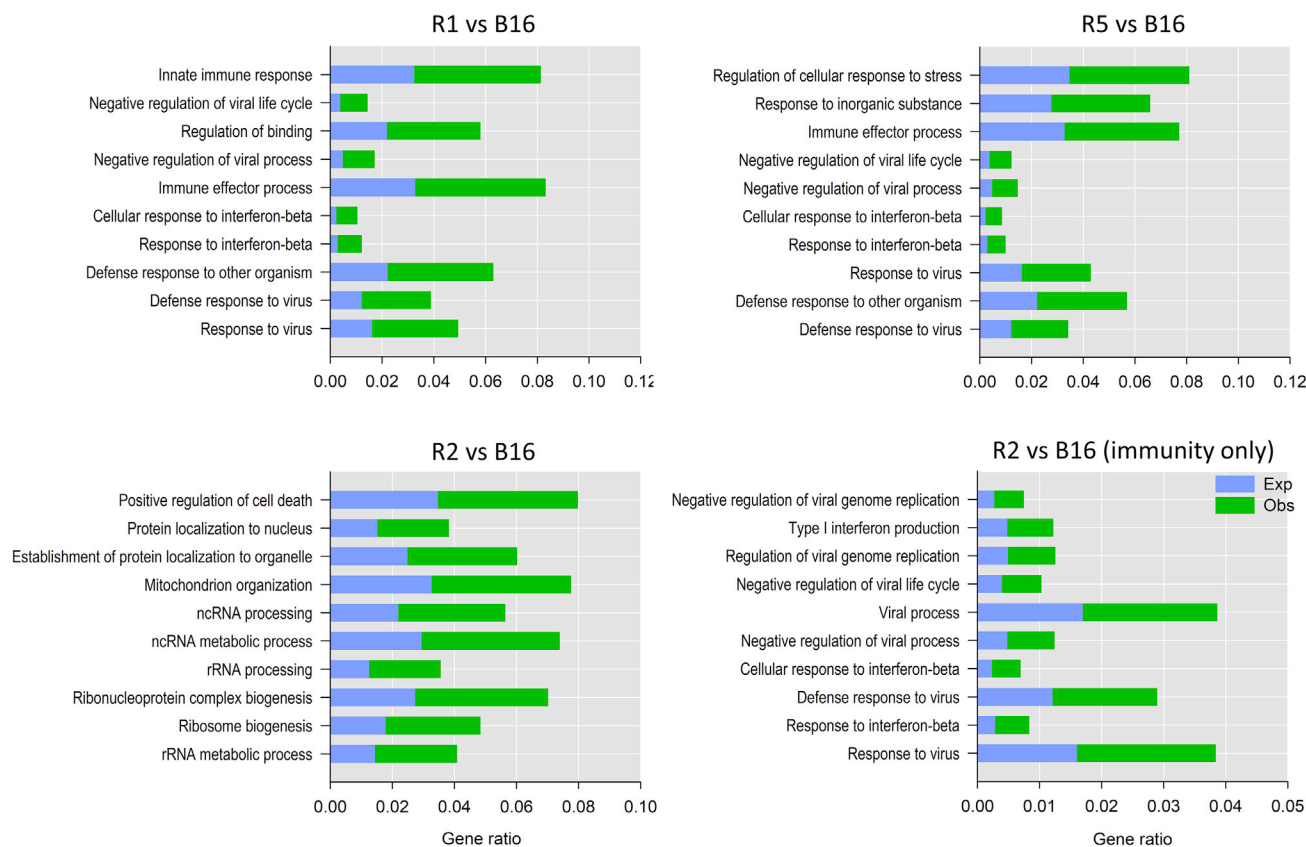


Figure 5. Gene ontology analysis comparing resistant and naïve B16 cells

Functional classes showing the 10 highest enrichment processes according to gene ratios are shown. In the fourth panel, the sub-class of pathways involved in immunity is shown separately for the R2-B16 comparison. Obs: observed ratio, Exp: expected ratio.

Selection of VSV-resistant CT26 carcinoma mouse cells can involve changes in gene expression resembling those found in B16 melanoma cells

To examine the generality of the gene expression remodeling experienced by VSV-resistant B16 cells, we used the same protocols to isolate two resistant clones (C1, C4) derived from the CT26 mouse carcinoma cell line. As above, resistance was tested by inoculating the selected clones with VSV-D51 at low MOI (0.1 PFU/cell) and monitoring fluorescence (Figure 7A), endpoint viral titer (24hpi, Figure 7B) and viral RNA at 8 hpi (Figure 7C). As opposed to B16, CT26 cells achieved only moderate levels of resistance to VSV. RNA-seq showed clearly differentiated gene expression profiles between clones C1 and C4, as well as between these clones and naïve cells (Figure 7D). Of interest, though, the C1 clone shared 397 overexpressed genes with the three resistant B16 clones R1, R2 and R5, and the overall changes in gene expression shown by this clone were significantly correlated with those exhibited by R1, R2 and R5 (Pearson $r > 0.65$; Figure 7E). The top 50 overexpressed genes shared between R1, R2 and R5 were also strongly overexpressed in C1 (Table S5). GO analysis of differentially expressed genes again revealed enrichment in pathways related to antiviral immune response (Figure 7F). These results suggest that sustained activation of immune response mechanisms in the absence of infection might be a general resistance mechanism in tumoral cells challenged with oncolytic VSV. However, clone C4 showed no similarities in gene expression changes with any of the VSV-resistant B16 clones, Table S5, as well as weak correlation with C1, suggesting the involvement of alternative resistant mechanisms (Figure S5).

DISCUSSION

Oncolytic VSV tropism towards tumor cells is largely driven by the predisposition to viral infection that these cells acquire following inactivation of immune responses, particularly those related to type-I IFNs.^{49,50} Thus, variations in IFN responsiveness across cells can limit treatment efficacy.³¹ Here, we have

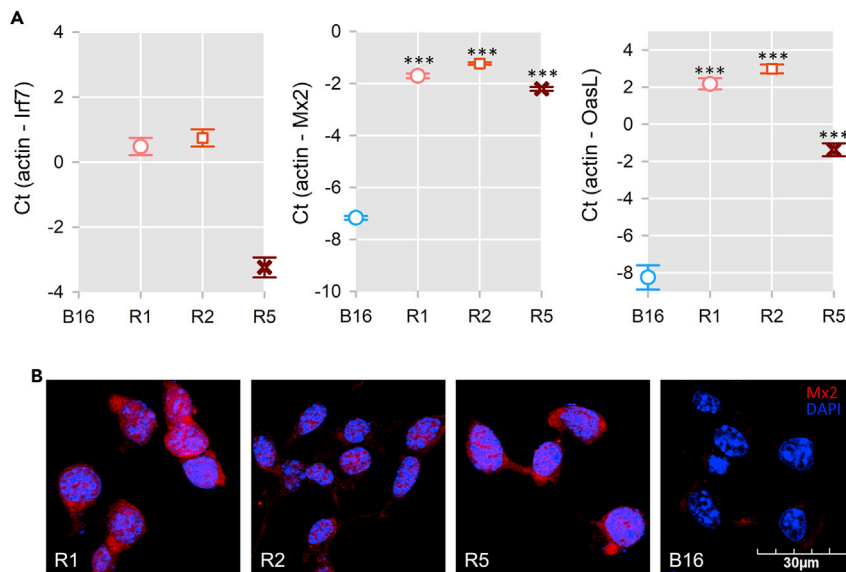


Figure 6. Validation of RNA-seq results by RT-qPCR and immunofluorescence

(A) RT-qPCR analysis of constitutive *Irf7*, *Mx2* and *Oasl* expression in naïve B16 and selected clones. Asterisks indicate significant differences with naïve B16 cells. *** $p < 0.001$, by a *t*-test. Statistical comparison could not be performed for *Irf7* because mRNA was not detected in naïve B16 cells. Data are presented as mean \pm SEM.

(B) Immunofluorescence microscopy showing *Mx2* expression (red: anti-Mx1/2/3; blue: DAPI).

directionally selected for VSV-resistant clones in B16 melanoma cells, and we have investigated the mechanisms underlying the emergence of resistance. We found that cells infected with VSV-D51 rapidly became refractory to infection, whereas WT VSV caused massive cell death with no cell population regrowth. RNA-seq data showed that chronic activation of multiple genes involved in innate immunity was a common theme in the selected resistant cells. This change in gene expression patterns conferred resistance to VSV-D51, but also to WT VSV and to an RNA virus from a different family (Sindbis virus). These results are consistent with previously published works, which describe that chronic activation of IFN pathways may play a role in long-term resistance to different cancer treatments, including oncolytic viruses.^{31,38,51–58} However, we did not find evidence that intercellular cytokine-mediated antiviral signaling could be chronically activated in the selected resistant clones. Although the expression of type-I IFN genes (*Ifnb1* and *Ifna4*) was slightly activated in R1 and R5 clones, our assays indicate that this was probably not sufficient to induce a significant paracrine response. Activation of these IFN genes was expected because they are also under the control of other ISGs as part of a positive feedback regulation.

Most of the top 50 genes overexpressed in resistant clones have some described antiviral function according to the Interferome database.⁵⁹ Some of these antiviral genes have been previously shown to be markers of VSV resistance. For instance, Mx GTPases are known to be important antiviral proteins genes against VSV and other viruses,⁴⁰ and their constitutive expression has been observed in VSV-resistant sarcoma SW982 cells.^{38,60} It has also been reported that 3T3 mouse cells overexpressing Mx1 show a high degree of resistance to VSV.⁶¹ Furthermore, MxA (Mx1 orthologue) and OAS proteins have been identified in previous studies as resistance markers to VSV-D51 infection in human pancreatic ductal adenocarcinoma cells (PDAC)^{37,38} and CT26 cells.³¹ In turn, constitutive OAS expression has been observed in VSV-resistant human mesothelioma cells,⁵⁵ as well as in PDAC.³⁷ Overexpression of other ISGs such as *Irf7* has been previously detected in VSV-resistant PDAC.³⁸ IFIT proteins,^{62–65} which block virus entry via endosomes and lysosomes⁶⁶ and bind specifically to viral mRNAs to prevent translation,⁶⁷ are other well-known ISGs that were upregulated in our resistant clones. We also found strong overexpression of certain tripartite-motif (TRIM) family members (*Trim12c*, *Trim30*, and *Trim34*), which play an important role against certain viruses such as human immunodeficiency virus (HIV)^{66,68,69} but have not been previously implicated in cellular resistance to VSV or oncolytic viruses. Finally, interferon-inducible GTPase 1 (*Iigp1*) was also highly overexpressed. This protein suppresses replication of the related rabies virus by blocking viral phosphoprotein dimerization.⁷⁰ There are currently hundreds of IFN-stimulated genes described,^{66,71} many of them

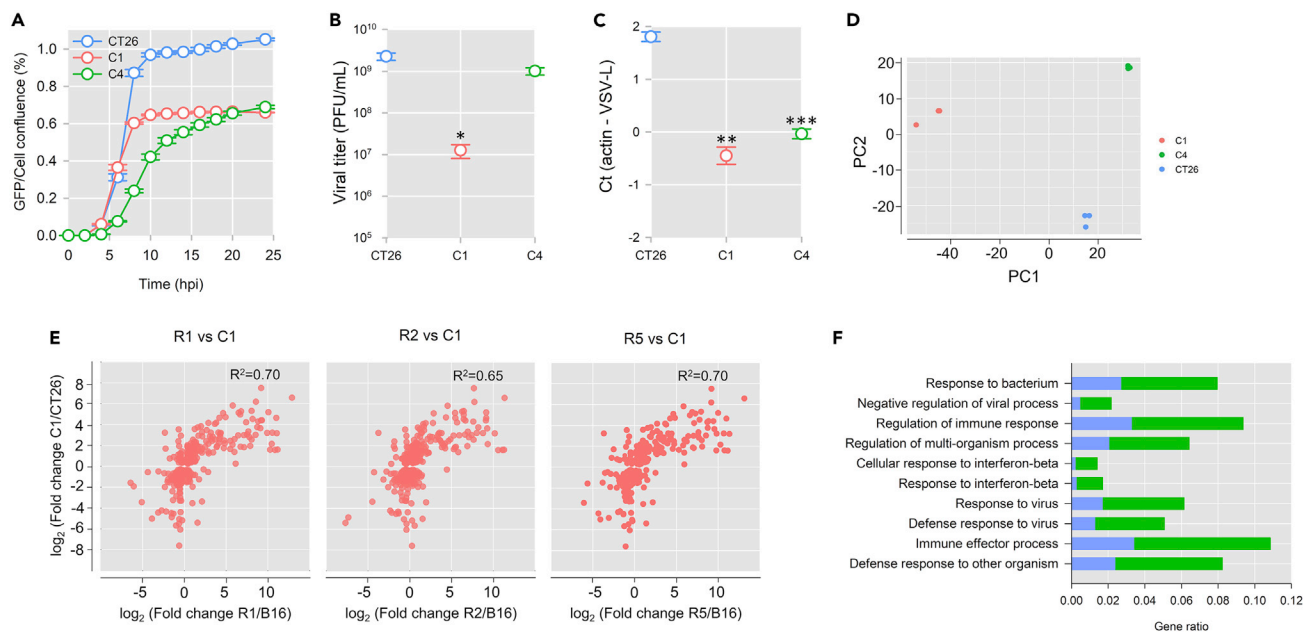


Figure 7. Characterization and analysis of VSV-resistant CT26-derived clones

(A) Infection spread tracking by real-time live-cell fluorescence microscopy in naïve CT26 cells and resistant clones C1 and C4 after infection with VSV-D51 (MOI = 0.1 PFU/cell).

(B) Viral production progeny after 24hpi. Significant differences by t-test are marked with asterisks (***) $p < 0.001$; ** $p < 0.01$.

(C) RT-qPCR analysis of viral RNA (RNA-L) produced in cells inoculated at low MOI (0.1 PFU/cell) after 8 hpi. Data are presented as mean \pm SEM.

(D) Principal component analysis of global gene expression in resistant C1, C4, and naïve CT26 cells.

(E) Correlation between differential gene expression values in the resistant C1 clone and each of the three B16 resistant clones (R1, R2 and R5).

(F) Gene ontology analysis of the 10 highest enrichment processes comparing C1 and naïve CT26 cells. Green: observed ratio, Blue: expected ratio.

significantly overexpressed in our B16 resistant clones, which makes it very likely that the observed resistance involved much more than overexpression of these few previously described genes.

In contrast, we found no evidence that resistance could be mediated by loss of viral attachment, because expression of low-density lipoprotein receptor gene (*Ldlr*), the principal cell receptor for VSV⁷² was detected in all resistant clones, and was even slightly elevated compared to naïve B16 cells (\log_2 fold changes of 0.34, 0.28 and 0.27; $p < 0.01$ in R1, R2 and R5 respectively). Alternative receptors, such as the low-density lipoprotein receptor class A Domain (*Ldlrad*) were similarly expressed in naïve and resistant cells. We also found an enrichment in endocytosis GO pathways in resistant clones both in early (GO:0005769), late endosomes (GO:0005770), and complete endocytosis processes (GO:0006897), suggesting that post-attachment VSV entry processes were not shut down in resistant cells.

Resistant clones showed a strong overexpression of genes whose antiviral function was less clear. For instance, the three Sp100 family members (*Sp100*, *Sp110* and *Sp140*) were overexpressed in resistant clones. These proteins are chromatin “readers” implicated in immunity disorders. Sp100 has been described as a regulator of some human DNA viruses,^{73,74} but their role in defense against viral RNA infection has not been clearly elucidated, and it is not known whether these proteins restrict viruses by regulating viral or host transcription.⁷⁵ Several members of the P200 family (HIN-200 in humans) were also among the top-50 overexpressed genes (*Mnda*, *Mndal*, *Ifi44*, *Ifi203*, *Ifi204*, *Ifi206* and *Ifi207*). This family of proteins participate in various cellular functions,^{76–78} including modulation of innate immunity after RNA virus infection to avoid hyper-inflammatory responses.⁷⁷ However, none of these proteins have been associated with resistance to VSV. Another highly overexpressed genes were *Psm8* and *Psm9*, which encode immunoproteasome subunits⁷⁹ but have no known role against VSV or related viruses. *Olf56*, which encodes a mouse olfactory receptor, was highly upregulated not only in resistant B16 but also in the C1 CT26 clone.

Our results also revealed the overexpression of 129, 150 and 347 non-coding RNAs in R1, R2 and R5, respectively. *C130026l21Rik* lncRNA, which is known to be produced following IFN secretion,^{80,81} was highly

overexpressed in R1 and R5. The involvement of this and other long non-coding RNAs in modulating resistance to VSV is unknown, though. However, the participation of long non-coding RNAs in immune regulation is being increasingly recognized.^{82–84} For instance, *lncRNA-COX2* has been identified as an important regulator of the immune response in human TLR-activated macrophages, and its rapid upregulation controls a large number of ISGs and NFκB-regulated genes.⁸⁵

We also found that 29 of the 50 most under-expressed genes in our B16 resistant clones were somewhat related to immunity according to the Interferome database. However, their role in oncolytic virus resistance is largely unknown, and we can provide at present no explanation for their under-expression, aside from speculating that they could be involved in modulating a chronic antiviral state. For instance, *Btn2a2* and potassium-channel subfamily K member 5 (*Kcnk5*), which were under-expressed in the three resistant clones, have been shown to participate in T-cell mediated immunity.^{48,86} Microtubule-associated protein 1A (*Map1a*) and carnitine palmitoyltransferase 1C (*Cpt1c*) promote HIV-1 routing to the nucleus and viral replication.^{87,88} Carbonyl Reductase 1 (*Cbr1*) is an anti-inflammatory mediator,⁸⁹ Phosphoinositide-3-Kinase regulatory subunit 5 (*Pik2r5*) is an inflammation-related gene with a prognostic value for lung adenocarcinoma,^{90,91} and cardiostrophin 1 (*Ctf1*) an immune-related gene belonging to the IL-6 family.⁹² However, none of these genes has been described to participate in the VSV infection cycle, or has been associated with oncolytic virus infection outcomes.

Overall, we found a remarkably high correlation between the differential gene expression patterns shown by the three B16 resistant clones examined. Considering the high number of cells that survived the initial challenge with VSV-D51, it is unlikely that three clones were derived from the same initial surviving cell, meaning that they probably represent independent resistance acquisition events. In addition, correlated differential gene expression patterns were obtained in one of the two VSV-resistant clones isolated from CT26 mouse carcinoma cells, an unrelated tumor cell line. The reproducibility shown by gene expression shifts supports the hypothesis that chronic activation of innate immunity genes is a potentially predictable cellular response to oncolytic virus treatment. However, differences between R2 and R1/R5 B16 clones and between C1 and C4 CT26 clones revealed alternative resistance mechanisms, and several genes with unknown antiviral function were strongly overexpressed in these resistant cells.

Technologies such as RNA interference (RNAi), short interfering RNA (siRNA), short hairpin RNA (shRNA), and CRISPR-Cas have been extensively used in the last decade to experimentally disrupt gene expression and identify host factors required by viruses for successful infection.^{93–99} Similar to other transcriptomic analyses, our study thus provides a number of candidate markers with known mechanisms of action, but also suggests new viral resistance targets that deserve in-depth examination in future work using the above techniques. The study of cellular resistances to other oncolytic viruses could be useful for identifying common resistance markers in future work. Likewise, selection of resistant cells derived directly from patients would be an interesting approach, because this would allow contrasting our results in a biomedically more relevant setting.

Limitations of the study

The gene expression patterns associated to VSV resistance were observed in two murine cell lines. Their generality remains to be tested further using additional cell lines from mice and other species, including humans. This may provide good candidate genes to uncover novel antiviral pathways, which could be validated using siRNA or overexpression experiments. Our results suggest that inhibition of VSV entry was not a major resistance mechanism in B16 and CT26 cells, but this conclusion remains to be validated experimentally.

STAR★METHODS

Detailed methods are provided in the online version of this paper and include the following:

- [KEY RESOURCES TABLE](#)
- [RESOURCE AVAILABILITY](#)
 - Lead contact
 - Materials availability
 - Data and code availability
- [METHOD DETAILS](#)
 - Virus strains

- Cell lines and culture
- Viral titration by plaque assay
- Automated real-time fluorescence microscopy
- Cell sorting and clonal expansion
- RNA extraction, cDNA synthesis and quantitative PCR
- Preparation of conditioned media
- RNA extraction, quantitation, and integrity analysis for RNA sequencing
- cDNA library preparation and Illumina RNA sequencing
- Gene expression quantitation and differential expression analysis
- Enrichment analyses
- STRING protein-protein interaction analysis
- Immunofluorescence and confocal microscopy images
- **QUANTIFICATION AND STATISTICAL DETAILS**

SUPPLEMENTAL INFORMATION

Supplemental information can be found online at <https://doi.org/10.1016/j.isci.2022.105749>.

ACKNOWLEDGMENTS

We thank Ramón Alemany for helpful comments, Pilar Domingo-Calap for help with resistant cell isolation, and María Durán-Moreno and Juan Vicente Bou for technical assistance. This work was supported by grant BFU2017-84762 from the Ministerio de Ciencia e Innovación to R.S.

AUTHOR CONTRIBUTIONS

Conceptualization, R.S.; Methodology, A.L. and R.S.; Investigation, A.L.; Resources, R.S.; Writing – Original Draft, A.L. and R.S.; Visualization, A.L. and R.S.; Supervision, R.S.; Funding acquisition, R.S.

DECLARATION OF INTERESTS

The authors declare no competing interests.

Received: April 29, 2022

Revised: September 23, 2022

Accepted: December 2, 2022

Published: January 20, 2023

REFERENCES

1. Kaufman, H.L., Kohlhapp, F.J., and Zloza, A. (2015). Oncolytic viruses: a new class of immunotherapy drugs. *Nat. Rev. Drug Discov.* *14*, 642–662. <https://doi.org/10.1038/nrd4663>.
2. Seegers, S.L., Frasier, C., Greene, S., Nesselova, I.V., and Grdzlishvili, V.Z. (2020). Experimental evolution generates novel oncolytic vesicular stomatitis viruses with improved replication in virus-resistant pancreatic cancer cells. *J. Virol.* *94*, 016433–19. <https://doi.org/10.1128/jvi.01643-19>.
3. Barber, G.N. (2001). Host defense, viruses and apoptosis. *Cell Death Differ.* *8*, 113–126. <https://doi.org/10.1038/sj.cdd.4400823>.
4. Huff, A.L., Wongthida, P., Kotte, T., Thompson, J.M., Driscoll, C.B., Schuelke, M., Shim, K.G., Harris, R.S., Molan, A., Pulido, J.S., et al. (2018). APOBEC3 mediates resistance to oncolytic viral therapy. *Mol. Ther. Oncolytics* *11*, 1–13. <https://doi.org/10.1016/j.omto.2018.08.003>.
5. Sobhanimonfared, F., Bamdad, T., Sadigh, Z.A., and Choobin, H. (2020). Virus specific tolerance enhanced efficacy of cancer immuno-virotherapy. *Microb. Pathog.* *140*, 103957. <https://doi.org/10.1016/j.micpath.2019.103957>.
6. Fouad, Y.A., and Aanei, C. (2017). Revisiting the hallmarks of cancer. *Am. J. Cancer Res.* *7*, 1016–1036.
7. Hanahan, D., and Weinberg, R.A. (2011). Hallmarks of cancer: the next generation. *Cell* *144*, 646–674. <https://doi.org/10.1016/j.cell.2011.02.013>.
8. Bhatt, D.K., Chammas, R., and Daemen, T. (2021). Resistance mechanisms influencing oncolytic virotherapy, a systematic analysis. *Vaccines* *9*, 1166. <https://doi.org/10.3390/vaccines9101166>.
9. Buijs, P.R.A., Verhagen, J.H.E., van Eijck, C.H.J., and van den Hoogen, B.G. (2015). Oncolytic viruses: from bench to bedside with a focus on safety. *Hum. Vaccines Immunother.* *11*, 1573–1584. <https://doi.org/10.1080/21645515.2015.1037058>.
10. Ebrahimi, S., Ghorbani, E., Khazaei, M., Avan, A., Ryzhikov, M., Azadmanesh, K., and Hassanian, S.M. (2017). Interferon-mediated tumor resistance to oncolytic virotherapy. *J. Cell. Biochem.* *118*, 1994–1999. <https://doi.org/10.1002/jcb.25917>.
11. Bieler, A., Mantwill, K., Dravits, T., Bernshausen, A., Glockzin, G., Köhler-Vargas, N., Lage, H., Gansbacher, B., and Holm, P.S. (2006). Novel three-pronged strategy to enhance cancer cell killing in glioblastoma cell lines: histone deacetylase inhibitor, chemotherapy, and oncolytic adenovirus dl520. *Hum. Gene Ther.* *17*, 55–70. <https://doi.org/10.1089/hum.2006.17.55>.
12. Selman, M., Ou, P., Rousso, C., Bergeron, A., Krishnan, R., Pikor, L., Chen, A., Keller, B.A., Ilkow, C., Bell, J.C., and Diallo, J.S. (2018). Dimethyl fumarate potentiates oncolytic virotherapy through NF-κB inhibition. *Sci. Transl. Med.* *10*, eaao1613. <https://doi.org/10.1126/scitranslmed.aao1613>.

13. Shulak, L., Beljanski, V., Chiang, C., Dutta, S.M., Van Grevenynghe, J., Belgnaoui, S.M., Nguyen, T.L.A., Di Lenardo, T., Semmes, O.J., Lin, R., and Hiscott, J. (2014). Histone deacetylase inhibitors potentiate vesicular stomatitis virus oncolysis in prostate cancer cells by modulating NF- κ B-Dependent autophagy. *J. Virol.* **88**, 2927–2940. <https://doi.org/10.1128/jvi.03406-13>.
14. Reinblatt, M., Pin, R.H., Federoff, H.J., and Fong, Y. (2004). Utilizing tumor hypoxia to enhance oncolytic viral therapy in colorectal metastases. *Ann. Surg.* **239**, 892–899. <https://doi.org/10.1097/01.sla.0000128308.36393.38>.
15. Evgin, L., Huff, A.L., Kottke, T., Thompson, J., Molan, A.M., Driscoll, C.B., Schuelke, M., Shim, K.G., Wongthida, P., Ilett, E.J., et al. (2019). Suboptimal T-cell therapy drives a tumor cell mutator phenotype that promotes escape from first-line treatment. *Cancer Immunol. Res.* **7**, 828–840. <https://doi.org/10.1158/2326-6066.CIR-18-0013>.
16. Choi, A.H., O’Leary, M.P., Lu, J., Kim, S.-I., Fong, Y., and Chen, N.G. (2018). Endogenous akt activity promotes virus entry and predicts efficacy of novel chimeric orthopoxvirus in triple-negative breast cancer. *Mol. Ther. Oncolytics* **9**, 22–29. <https://doi.org/10.1016/j.omto.2018.04.001>.
17. Tong, J.G., Valdes, Y.R., Sivapragasam, M., Barrett, J.W., Bell, J.C., Stojdl, D., DiMattia, G.E., and Shepherd, T.G. (2017). Spatial and temporal epithelial ovarian cancer cell heterogeneity impacts Maraba virus oncolytic potential. *BMC Cancer* **17**, 594. <https://doi.org/10.1186/s12885-017-3600-2>.
18. Tseng, J.C., Granot, T., Digiacomio, V., Levin, B., and Meruelo, D. (2010). Enhanced specific delivery and targeting of oncolytic Sindbis viral vectors by modulating vascular leakiness in tumor. *Cancer Gene Ther.* **17**, 244–255. <https://doi.org/10.1038/cgt.2009.70>.
19. Valyi-Nagy, K., Dosa, S., Kovacs, S.K., Bacsa, S., Voros, A., Shukla, D., Folberg, R., and Valyi-Nagy, T. (2010). Identification of virus resistant tumor cell subpopulations in three-dimensional uveal melanoma cultures. *Cancer Gene Ther.* **17**, 223–234. <https://doi.org/10.1038/cgt.2009.73>.
20. Watanabe, Y., Kojima, T., Kagawa, S., Uno, F., Hashimoto, Y., Kyo, S., Mizuguchi, H., Tanaka, N., Kawamura, H., Ichimaru, D., et al. (2010). A novel translational approach for human malignant pleural mesothelioma: heparanase-assisted dual virotherapy. *Oncogene* **29**, 1145–1154. <https://doi.org/10.1038/onc.2009.415>.
21. Yumul, R., Richter, M., Lu, Z.Z., Saydaminova, K., Wang, H., Wang, C.H.K., Carter, D., and Lieber, A. (2016). Epithelial junction opener improves oncolytic adenovirus therapy in mouse tumor models. *Hum. Gene Ther.* **27**, 325–337. <https://doi.org/10.1089/hum.2016.022>.
22. Cataldi, M., Shah, N.R., Felt, S.A., and Grdzlishvili, V.Z. (2015). Breaking resistance of pancreatic cancer cells to an attenuated vesicular stomatitis virus through a novel activity of IKK inhibitor TPCA-1. *Virology* **485**, 340–354. <https://doi.org/10.1016/j.virol.2015.08.003>.
23. Hoang, H.-D., Graber, T.E., Jia, J.-J., Vaidya, N., Gilchrist, V.H., Xiang, X., Li, W., Cowan, K.N., Gkogkas, C.G., Jaramillo, M., et al. (2019). Induction of an Alternative mRNA 5’ Leader Enhances Translation of the Ciliopathy Gene Inpp5e and Resistance to Oncolytic Virus Infection. *Cell Rep.* **29**, 4010–4023.e5. <https://doi.org/10.1016/j.celrep.2019.11.072>.
24. Gholami, S., Chen, C.-H., Gao, S., Lou, E., Fujisawa, S., Carson, J., Nnoli, J.E., Chou, T.-C., Bromberg, J., and Fong, Y. (2014). Role of MAPK in oncolytic herpes viral therapy in triple-negative breast cancer. *Cancer Gene Ther.* **21**, 283–289. <https://doi.org/10.1038/cgt.2014.28>.
25. Su, B.-H., Shieh, G.-S., Tseng, Y.-L., Shiau, A.-L., and Wu, C.-L. (2015). Etoposide enhances antitumor efficacy of MDR1-driven oncolytic adenovirus through autoupregulation of the MDR1 promoter activity. *Oncotarget* **6**, 38308–38326. <https://doi.org/10.18632/oncotarget.5702>.
26. Bommareddy, P.K., Aspromonte, S., Zloza, A., Rabkin, S.D., and Kaufman, H.L. (2018). MEK inhibition enhances oncolytic virus immunotherapy through increased tumor cell killing and T cell activation. *Sci. Transl. Med.* **10**, eaau0417. <https://doi.org/10.1126/scitranslmed.aau0417>.
27. Dobson, C.C., Naing, T., Beug, S.T., Faye, M.D., Chabot, J., St-Jean, M., Walker, D.E., LaCasse, E.C., Stojdl, D.F., Korneluk, R.G., and Holcik, M. (2017). Oncolytic virus synergizes with Smac mimetic compounds to induce rhabdomyosarcoma cell death in a syngeneic murine model. *Oncotarget* **8**, 3495–3508. <https://doi.org/10.18632/oncotarget.13849>.
28. Li, W., Turaga, R.C., Li, X., Sharma, M., Enadi, Z., Dunham Tompkins, S.N., Hardy, K.C., Mishra, F., Tsao, J., Liu, Z.R., et al. (2019). Overexpression of smac by an armed vesicular stomatitis virus overcomes tumor resistance. *Mol. Ther. Oncolytics* **14**, 188–195. <https://doi.org/10.1016/j.omto.2019.05.006>.
29. Muscolini, M., Castiello, L., Palermo, E., Zevini, A., Ferrari, M., Olgner, D., and Hiscott, J. (2019). SIRT1 modulates the sensitivity of prostate cancer cells to vesicular stomatitis virus oncolysis. *J. Virol.* **93**, 006266-19. <https://doi.org/10.1128/JVI.00626-19>.
30. Li, Y., Zhuo, B., Yin, Y., Han, T., Li, S., Li, Z., and Wang, J. (2017). Anti-cancer effect of oncolytic adenovirus-armed shRNA targeting MYCN gene on doxorubicin-resistant neuroblastoma cells. *Biochem. Biophys. Res. Commun.* **491**, 134–139. <https://doi.org/10.1016/j.bbrc.2017.07.062>.
31. Ruotsalainen, J.J., Kaikkonen, M.U., Niittikoski, M., Martikainen, M.W., Lemay, C.G., Cox, J., De Silva, N.S., Kus, A., Falls, T.J., Diallo, J.S., et al. (2015). Clonal variation in interferon response determines the outcome of oncolytic virotherapy in mouse CT26 colon carcinoma model. *Gene Ther.* **22**, 65–75. <https://doi.org/10.1038/gt.2014.83>.
32. Hastie, E., and Grdzlishvili, V.Z. (2012). Vesicular stomatitis virus as a flexible platform for oncolytic virotherapy against cancer. *J. Gen. Virol.* **93**, 2529–2545. <https://doi.org/10.1099/vir.0.046672-0>.
33. Hastie, E., Cataldi, M., Marriott, I., and Grdzlishvili, V.Z. (2013). Understanding and altering cell tropism of vesicular stomatitis virus. *Virus Res.* **176**, 16–32. <https://doi.org/10.1016/j.virusres.2013.06.003>.
34. Stojdl, D.F., Lichty, B.D., tenOever, B.R., Paterson, J.M., Power, A.T., Knowles, S., Marius, R., Reynard, J., Poliquin, L., Atkins, H., et al. (2003). VSV strains with defects in their ability to shutdown innate immunity are potent systemic anti-cancer agents. *Cancer Cell* **4**, 263–275. [https://doi.org/10.1016/S1535-6108\(03\)00241-1](https://doi.org/10.1016/S1535-6108(03)00241-1).
35. Rieder, M., and Conzelmann, K.K. (2009). Rhabdovirus evasion of the interferon system. *J. Interferon Cytokine Res.* **29**, 499–509. <https://doi.org/10.1089/jir.2009.0068>.
36. Gregg, R.K. (2021). Model systems for the study of malignant melanoma. *Methods Mol. Biol.* **2265**, 1–21. https://doi.org/10.1007/978-1-0716-1205-7_1.
37. Hastie, E., Cataldi, M., Moerdyk-Schauwecker, M.J., Felt, S.A., Steuerwald, N., and Grdzlishvili, V.Z. (2016). Novel biomarkers of resistance of pancreatic cancer cells to oncolytic vesicular stomatitis virus. *Oncotarget* **7**, 61601–61618. <https://doi.org/10.18632/oncotarget.11202>.
38. Moerdyk-Schauwecker, M., Shah, N.R., Murphy, A.M., Hastie, E., Mukherjee, P., and Grdzlishvili, V.Z. (2013). Resistance of pancreatic cancer cells to oncolytic vesicular stomatitis virus: role of type I interferon signaling. *Virology* **436**, 221–234. <https://doi.org/10.1016/j.virol.2012.11.014>.
39. Hur, S. (2019). Double-stranded RNA sensors and modulators in innate immunity. *Annu. Rev. Immunol.* **37**, 349–375. <https://doi.org/10.1146/annurev-immunol-042718>.
40. Haller, O., Staeheli, P., Schwemmler, M., and Kochs, G. (2015). Mx GTPases: dynamin-like antiviral machines of innate immunity. *Trends Microbiol.* **23**, 154–163. <https://doi.org/10.1016/j.tim.2014.12.003>.
41. Mogensen, T.H. (2018). IRF and STAT transcription factors - from basic biology to roles in infection, protective immunity, and primary immunodeficiencies. *Front. Immunol.* **9**, 3047. <https://doi.org/10.3389/fimmu.2018.03047>.
42. Zhou, X., Michal, J.J., Zhang, L., Ding, B., Lunney, J.K., Liu, B., and Jiang, Z. (2013). Interferon induced IFIT family genes in host antiviral defense. *Int. J. Biol. Sci.* **9**, 200–208. <https://doi.org/10.7150/ijbs.5613>.
43. Kreit, M., Paul, S., Knoops, L., De Cock, A., Sorgeloos, F., and Michiels, T. (2014). Inefficient type I interferon-mediated antiviral protection of primary mouse neurons is associated with the lack of apolipoprotein L9 expression. *J. Virol.* **88**, 3874–3884. <https://doi.org/10.1128/jvi.03018-13>.

44. Kreit, M., Vertommen, D., Gillet, L., and Michiels, T. (2015). The interferon-inducible mouse apolipoprotein L9 and prohibitins cooperate to restrict Theiler's virus replication. *PLoS One* 10, e0133190. <https://doi.org/10.1371/journal.pone.0133190>.
45. Arvind, T.A., and Rangarajan, P.N. (2016). Mouse Apolipoprotein L9 is a phosphatidylethanolamine-binding protein. *Biochem. Biophys. Res. Commun.* 479, 636–642. <https://doi.org/10.1016/j.bbrc.2016.09.161>.
46. Fan, X., Jiao, L., and Jin, T. (2021). Activation and immune regulation mechanisms of PYHIN family during microbial infection. *Front. Microbiol.* 12, 809412. <https://doi.org/10.3389/fmicb.2021.809412>.
47. Gu, L., Casserly, D., Brady, G., Carpenter, S., Bracken, A.P., Fitzgerald, K.A., Unterholzner, L., and Bowie, A.G. (2022). Myeloid cell nuclear differentiation antigen controls the pathogen-stimulated type I interferon cascade in human monocytes by transcriptional regulation of IRF7. *Nat. Commun.* 13, 14. <https://doi.org/10.1038/s41467-021-27701-x>.
48. Sarter, K., Leimgruber, E., Gobet, F., Agrawal, V., Dunand-Sauthier, I., Barras, E., Mastelic-Gavillet, B., Kamath, A., Fontannaz, P., Guéry, L., et al. (2016). Btn2a2, a T cell immunomodulatory molecule coregulated with MHC class II genes. *J. Exp. Med.* 213, 177–187. <https://doi.org/10.1084/jem.20150435>.
49. Bishnoi, S., Tiwari, R., Gupta, S., Byrareddy, S.N., and Nayak, D. (2018). Oncotargeting by vesicular stomatitis virus (VSV): advances in cancer therapy. *Viruses* 10, 90. <https://doi.org/10.3390/v10020090>.
50. Felt, S.A., and Grdzlishvili, V.Z. (2017). Recent advances in vesicular stomatitis virus-based oncolytic virotherapy: a 5-year update. *J. Gen. Virol.* 98, 2895–2911. <https://doi.org/10.1099/jgv.0.000980>.
51. Budhwani, M., Mazzei, R., and Dolcetti, R. (2018). Plasticity of type I interferon-mediated responses in cancer therapy: from anti-tumor immunity to resistance. *Front. Oncol.* 8, 322. <https://doi.org/10.3389/fonc.2018.00322>.
52. Escobar-Zarate, D., Liu, Y.P., Suksanpaisan, L., Russell, S.J., and Peng, K.W. (2013). Overcoming cancer cell resistance to VSV oncolysis with JAK1/2 inhibitors. *Cancer Gene Ther.* 20, 582–589. <https://doi.org/10.1038/cgt.2013.55>.
53. Linge, C., Gewert, D., Rossmann, C., Bishop, J.A., and Crowe, J.S. (1995). Interferon system defects in human malignant melanoma. *Cancer Res.* 55, 4099–4104.
54. Naik, S., Nace, R., Federspiel, M.J., Barber, G.N., Peng, K.W., and Russell, S.J. (2012). Curative one-shot systemic virotherapy in murine myeloma. *Leukemia* 26, 1870–1878. <https://doi.org/10.1038/leu.2012.70>.
55. Saloura, V., Wang, L.-C.S., Fridlender, Z.G., Sun, J., Cheng, G., Kapoor, V., Sterman, D.H., Harty, R.N., Okumura, A., Barber, G.N., et al. (2010). Evaluation of an attenuated vesicular stomatitis virus vector expressing interferon- β for use in malignant pleural mesothelioma: heterogeneity in interferon responsiveness defines potential efficacy. *Hum. Gene Ther.* 21, 51–64. <https://doi.org/10.1089/hum.2009.088>.
56. Stojdl, D.F., Lichty, B., Knowles, S., Marius, R., Atkins, H., Sonenberg, N., and Bell, J.C. (2000). Exploiting tumor-specific defects in the interferon pathway with a previously unknown oncolytic virus. *Nat. Med.* 6, 821–825. <https://doi.org/10.1038/77558>.
57. Sun, W.H., Pabon, C., Alsayed, Y., Huang, P.P., Jandeska, S., Uddin, S., Platanias, L.C., and Rosen, S.T. (1998). Interferon- α resistance in a cutaneous T-cell lymphoma cell line is associated with lack of STAT1 expression. *Blood* 91, 570–576. <https://doi.org/10.1182/blood.v91.2.570>.
58. Wong, L.H., Krauer, K.G., Hatzinisiiriou, I., Estcourt, M.J., Hersey, P., Tam, N.D., Edmondson, S., Devenish, R.J., and Ralph, S.J. (1997). Interferon-resistant human melanoma cells are deficient in ISGF3 components, STAT1, STAT2, and p48-ISGF3 γ . *J. Biol. Chem.* 272, 28779–28785. <https://doi.org/10.1074/jbc.272.45.28779>.
59. Rusinova, I., Forster, S., Yu, S., Kannan, A., Masse, M., Cumming, H., Chapman, R., and Hertzog, P.J. (2013). INTERFEROME v2.0: an updated database of annotated interferon-regulated genes. *Nucleic Acids Res.* 41, D1040–D1046. <https://doi.org/10.1093/nar/gks1215>.
60. Paglino, J.C., and van den Pol, A.N. (2011). Vesicular stomatitis virus has extensive oncolytic activity against human sarcomas: rare resistance is overcome by blocking interferon pathways. *J. Virol.* 85, 9346–9358. <https://doi.org/10.1128/jvi.00723-11>.
61. Pavlovic, J., Zürcher, T., Haller, O., and Staeheli, P. (1990). Resistance to influenza virus and vesicular stomatitis virus conferred by expression of human MxA protein. *J. Virol.* 64, 3370–3375. <https://doi.org/10.1128/JVI.64.7.3370-3375.1990>.
62. Blondel, D., Maarifi, G., Nisole, S., and Chelbi-Alix, M.K. (2015). Resistance to rhabdoviridae infection and subversion of antiviral responses. *Viruses* 7, 3675–3702. <https://doi.org/10.3390/v7072794>.
63. Chai, B., Tian, D., Zhou, M., Tian, B., Yuan, Y., Sui, B., Wang, K., Pei, J., Huang, F., Wu, Q., et al. (2021). Murine ifit3 restricts the replication of rabies virus both in vitro and in vivo. *J. Gen. Virol.* 102, 001619. <https://doi.org/10.1099/JGV.0.001619>.
64. Davis, B.M., Fensterl, V., Lawrence, T.M., Hudacek, A.W., Sen, G.C., and Schnell, M.J. (2017). Ifit2 is a restriction factor in rabies virus pathogenicity. *J. Virol.* 91. <https://doi.org/10.1128/JVI.00889-17>.
65. Fensterl, V., Wetzel, J.L., Ramachandran, S., Ogino, T., Stohlman, S.A., Bergmann, C.C., Diamond, M.S., Virgin, H.W., and Sen, G.C. (2012). Interferon-induced Ifit2/ISG54 protects mice from lethal VSV neuropathogenesis. *PLoS Pathog.* 8, e1002712. <https://doi.org/10.1371/journal.ppat.1002712>.
66. Schneider, W.M., Chevillotte, M.D., and Rice, C.M. (2014). Interferon-stimulated genes: a complex web of host defenses. *Annu. Rev. Immunol.* 32, 513–545. <https://doi.org/10.1146/annurev-immunol-032713-120231>.
67. Fensterl, V., and Sen, G.C. (2015). Interferon-induced ift proteins: their role in viral pathogenesis. *J. Virol.* 89, 2462–2468. <https://doi.org/10.1128/jvi.02744-14>.
68. Shen, Z., Wei, L., Yu, Z.B., Yao, Z.Y., Cheng, J., Wang, Y.T., Song, X.T., and Li, M. (2021). The roles of TRIMs in antiviral innate immune signaling. *Front. Cell. Infect. Microbiol.* 11, 628275. <https://doi.org/10.3389/fcimb.2021.628275>.
69. Van Gent, M., Sparrer, K.M.J., and Gack, M.U. (2018). TRIM proteins and their roles in antiviral host defenses. *Annu. Rev. Virol.* 5, 385–405. <https://doi.org/10.1146/annurev-virology>.
70. Tian, B., Yuan, Y., Yang, Y., Luo, Z., Sui, B., Zhou, M., Fu, Z.F., and Zhao, L. (2020). Interferon-inducible GTPase 1 impedes the dimerization of rabies virus phosphoprotein and restricts viral replication. *J. Virol.* 94, e01203–e01220. <https://doi.org/10.1128/jvi.01203-20>.
71. Schoggins, J.W. (2019). Interferon-stimulated genes: what do they all do? *Annu. Rev. Virol.* 6, 567–584. <https://doi.org/10.1146/annurev-virology-092818>.
72. Finkelshtein, D., Werman, A., Novick, D., Barak, S., and Rubinstein, M. (2013). LDL receptor and its family members serve as the cellular receptors for vesicular stomatitis virus. *Proc. Natl. Acad. Sci. USA* 110, 7306–7311. <https://doi.org/10.1073/pnas.1214441110>.
73. Habiger, C., Jäger, G., Walter, M., Iftner, T., and Stubenrauch, F. (2016). Interferon kappa inhibits human papillomavirus 31 transcription by inducing Sp100 proteins. *J. Virol.* 90, 694–704. <https://doi.org/10.1128/JVI.02137-15>.
74. Stepp, W.H., Meyers, J.M., and McBride, A.A. (2013). Sp100 provides intrinsic immunity against human papillomavirus infection. *mBio* 4, 008455–e913. <https://doi.org/10.1128/mBio.00845-13>.
75. Fraschilla, I., and Jeffrey, K.L. (2020). The speckled protein (SP) family: immunity's chromatin readers. *Trends Immunol.* 41, 572–585. <https://doi.org/10.1016/j.it.2020.04.007>.
76. Asefa, B., Klarmann, K.D., Copeland, N.G., Gilbert, D.J., Jenkins, N.A., and Keller, J.R. (2004). The interferon-inducible p200 family of proteins: a perspective on their roles in cell cycle regulation and differentiation. *Blood Cells Mol. Dis.* 32, 155–167. <https://doi.org/10.1016/j.bcmd.2003.10.002>.
77. Cao, L., Ji, Y., Zeng, L., Liu, Q., Zhang, Z., Guo, S., Guo, X., Tong, Y., Zhao, X., Li, C.M., et al. (2019). P200 family protein IFI204 negatively regulates type I interferon responses by

- targeting IRF7 in nucleus. *PLoS Pathog.* 15, e1008079. <https://doi.org/10.1371/journal.ppat.1008079>.
78. Gariglio, M., Mondini, M., De Andrea, M., and Landolfo, S. (2011). The multifaceted interferon-inducible p200 family proteins: from cell biology to human pathology. *J. Interferon Cytokine Res.* 31, 159–172. <https://doi.org/10.1089/jir.2010.0106>.
 79. Kitamura, A., Maekawa, Y., Uehara, H., Izumi, K., Kawachi, I., Nishizawa, M., Toyoshima, Y., Takahashi, H., Standley, D.M., Tanaka, K., et al. (2011). A mutation in the immunoproteasome subunit PSMB8 causes autoinflammation and lipodystrophy in humans. *J. Clin. Invest.* 121, 4150–4160. <https://doi.org/10.1172/JCI58414>.
 80. De Weerd, N.A., Vivian, J.P., Nguyen, T.K., Mangan, N.E., Gould, J.A., Braniff, S.J., Zaker-Tabrizi, L., Fung, K.Y., Forster, S.C., Beddoe, T., et al. (2013). Structural basis of a unique interferon- β signaling axis mediated via the receptor IFNAR1. *Nat. Immunol.* 14, 901–907. <https://doi.org/10.1038/ni.2667>.
 81. Josset, L., Tchitchek, N., Gralinski, L.E., Ferris, M.T., Eisfeld, A.J., Green, R.R., Thomas, M.J., Tisoncik-Go, J., Schroth, G.P., Kawaoka, Y., et al. (2014). Annotation of long non-coding RNAs expressed in Collaborative Cross founder mice in response to respiratory virus infection reveals a new class of interferon-stimulated transcripts. *RNA Biol.* 11, 875–890. <https://doi.org/10.4161/ma.29442>.
 82. Carpenter, S. (2016). Long noncoding RNA: novel links between gene expression and innate immunity. *Virus Res.* 212, 137–145. <https://doi.org/10.1016/j.virusres.2015.08.019>.
 83. Robinson, E.K., Covarrubias, S., and Carpenter, S. (2020). The how and why of lncRNA function: an innate immune perspective. *Biochim. Biophys. Acta. Gene Regul. Mech.* 1863, 194419. <https://doi.org/10.1016/j.bbagr.2019.194419>.
 84. Carpenter, S., and Fitzgerald, K.A. (2018). Cytokines and long noncoding RNAs. *Cold Spring Harbor Perspect. Biol.* 10, a028589. <https://doi.org/10.1101/cshperspect.a028589>.
 85. Satpathy, A.T., and Chang, H.Y. (2015). Long noncoding RNA in hematopoiesis and immunity. *Immunity* 42, 792–804. <https://doi.org/10.1016/j.immuni.2015.05.004>.
 86. Kirkegaard, S.S., Strøm, P.D., Gammeltoft, S., Hansen, A.J., and Hoffmann, E.K. (2016). The volume activated potassium channel KCNK5 is up-regulated in activated human T Cells, but volume regulation is impaired. *Cell. Physiol. Biochem.* 38, 883–892. <https://doi.org/10.1159/000443042>.
 87. Corley, M.J., Pang, A.P.S., Rasmussen, T.A., Tolstrup, M., Søgaard, O.S., and Ndhlovu, L.C. (2021). Candidate host epigenetic marks predictive for HIV reservoir size, responsiveness to latency reversal, and viral rebound. *AIDS* 35, 2269–2279. <https://doi.org/10.1097/QAD.0000000000003065>.
 88. Fernandez, J., Portillo, D.M., Danckaert, A., Munier, S., Becker, A., Roux, P., Zambo, A., Shorte, S., Jacob, Y., Vidalain, P.O., et al. (2015). Microtubule-associated proteins 1 (MAP1) promote human immunodeficiency virus type 1 (HIV-1) intracytoplasmic routing to the nucleus. *J. Biol. Chem.* 290, 4631–4646. <https://doi.org/10.1074/jbc.M114.613133>.
 89. Kim, Y.N., Kim, D.W., Jo, H.S., Shin, M.J., Ahn, E.H., Ryu, E.J., Yong, J.I., Cha, H.J., Kim, S.J., Yeo, H.J., et al. (2015). Tat-CBR1 inhibits inflammatory responses through the suppressions of NF- κ B and MAPK activation in macrophages and TPA-induced ear edema in mice. *Toxicol. Appl. Pharmacol.* 286, 124–134. <https://doi.org/10.1016/j.taap.2015.03.020>.
 90. Liu, Z.J., Hou, P.X., and Wang, X.X. (2021). An inflammation-related nine-gene signature to improve prognosis prediction of lung adenocarcinoma. *Dis. Markers* 2021, 9568057. <https://doi.org/10.1155/2021/9568057>.
 91. Ye, Z.S., Zheng, M., Liu, Q.Y., Zeng, Y., Wei, S.H., Wang, Y., Lin, Z.T., Shu, C., Zheng, Q.H., and Chen, L.C. (2021). Survival-associated alternative splicing events interact with the immune microenvironment in stomach adenocarcinoma. *World J. Gastroenterol.* 27, 2871–2894. <https://doi.org/10.3748/wjg.v27.i21.2871>.
 92. Liu, J., Chen, X., Jiang, Y., and Cheng, W. (2020). Development of an immune gene prognostic classifier for survival prediction and respond to immunotherapy in endometrial cancer. *Int. Immunopharm.* 86, 106735. <https://doi.org/10.1016/j.intimp.2020.106735>.
 93. Kirby, E.N., Shue, B., Thomas, P.Q., and Beard, M.R. (2021). CRISPR tackles emerging viral pathogens. *Viruses* 13, 2157. <https://doi.org/10.3390/v13112157>.
 94. Lee, A.S.-Y., Burdeinick-Kerr, R., and Whelan, S.P.J. (2014). A genome-wide small interfering RNA screen identifies host factors required for vesicular stomatitis virus infection. *J. Virol.* 88, 8355–8360. <https://doi.org/10.1128/JVI.00642-14>.
 95. Li, Q., Brass, A.L., Ng, A., Hu, Z., Xavier, R.J., Liang, T.J., and Elledge, S.J. (2009). A genome-wide genetic screen for host factors required for hepatitis C virus propagation. *Proc. Natl. Acad. Sci. USA* 106, 16410–16415. <https://doi.org/10.1073/pnas.0907439106>.
 96. Li, J., Wang, Y., Wang, B., Lou, J., Ni, P., Jin, Y., Chen, S., Duan, G., and Zhang, R. (2022). Application of CRISPR/cas systems in the nucleic acid detection of infectious diseases. *Diagnostics* 12, 2455. <https://doi.org/10.3390/diagnostics12102455>.
 97. Martin, S., Chiramel, A.I., Schmidt, M.L., Chen, Y.-C., Whitt, N., Watt, A., Dunham, E.C., Shifflett, K., Traeger, S., Leske, A., et al. (2018). A genome-wide siRNA screen identifies a druggable host pathway essential for the Ebola virus life cycle. *Genome Med.* 10, 58. <https://doi.org/10.1186/s13073-018-0570-1>.
 98. Radoshitzky, S.R., Pegoraro, G., Chī, X.O., Dōng, L., Chiang, C.-Y., Jozwick, L., Clester, J.C., Cooper, C.L., Courier, D., Langan, D.P., et al. (2016). siRNA screen identifies trafficking host factors that modulate alphavirus infection. *PLoS Pathog.* 12, e1005466. <https://doi.org/10.1371/journal.ppat.1005466>.
 99. Perreira, J.M., Meraner, P., and Brass, A.L. (2016). Functional genomic strategies for elucidating human-virus interactions: will CRISPR knockout RNAi and haploid cells? *Adv. Virus Res.* 94, 1–51. <https://doi.org/10.1016/bs.avir.2015.11.001>.

STAR★METHODS

KEY RESOURCES TABLE

REAGENT or RESOURCE	SOURCE	IDENTIFIER
Antibodies		
Mouse Anti-Mx1 / 2 / 3 Monoclonal Antibody, Unconjugated, Clone C-1	Santa Cruz Biotechnology	Cat# sc-166412; RRID: AB_2147714
AffiniPure Fab Fragment Goat Anti-Mouse IgG (H + L) antibody	Jackson ImmunoResearch Labs	Cat# 115-007-003; RRID: AB_2338476
Goat anti-Mouse IgG (H + L) Highly Cross-Adsorbed Secondary Antibody, Alexa Fluor Plus 594	Thermo Fisher Scientific	Cat# A32742; RRID:AB_2762825
Bacterial and virus strains		
VSV-WT-mCherry	Dr. J.K. Rose (Yale University School of Medicine)	N/A
VSV-Δ51	Dr. V. Grdzlishvili (University of North Carolina)	N/A
Sindbis virus	Dr. Carla Saleh (Institut Pasteur de Paris)	N/A
Chemicals, peptides, and recombinant proteins		
RNAzol RT reagent solution	Sigma-Aldrich	Cat# R4533
NZY Reverse Transcriptase	NZYtech	Cat# MB124
PowerUP SYBR Green qPCR Master Mix	Applied Biosciences	Cat# A25780
ProLong Gold antifade reagent containing DAPI	Invitrogen	Cat# P10144
Deposited data		
Global gene expression of B16-F10 cells sensible and resistant to oncolytic VSV D51 virus	SRA (Sequence Read Archive)	PRJNA824679
Global gene expression of CT26 cells sensible and resistant to oncolytic VSV D51 virus	SRA (Sequence Read Archive)	PRJNA855353
Experimental models: Cell lines		
Mouse: CT26	ATCC	ATCC Cat# CRL-2639; RRID: CVCL_7255
Mouse: B16-F10	ATCC	ATCC Cat# CRL-6475; RRID: CVCL_0159
Hamster: BHK-21	ATCC	ATCC Cat# CCL-10; RRID: CVCL_1915
Oligonucleotides		
Primer: VSV gene L Forward AACGATTCCCCACAAGATCCC	This paper	N/A
Primer: VSV gene L Reverse GCAAGAGGGTGGTGAAATAGAG	This paper	N/A
Primer: VSV gene P Forward CGCCAGAGGGTTAAGTGAG	This paper	N/A
Primer: VSV gene P Reverse TTCTGATTGGGACGGATGTGTG	This paper	N/A
Primer: mouse Mx2 gene Forward ACACGGTCACTGAAATTGTACG	This paper	N/A
Primer: mouse Mx2 gene Reverse TGGAGTCGGATTGACATCTCTG	This paper	N/A

(Continued on next page)

Continued

REAGENT or RESOURCE	SOURCE	IDENTIFIER
Primer: mouse Irf7 gene Forward CCAGTTGATCCGCATAAGGT	This paper	N/A
Primer: mouse Irf7 gene Reverse GAGCCCAGCATTCTCTTG	This paper	N/A
Primer: mouse Oasl gene Forward TTGTGCGGAGGATCAGGTACT	This paper	N/A
Primer: mouse Oasl gene Reverse TGATGGTGTGCGCAGTCTTTGA	This paper	N/A
Primer: mouse Actin-b gene Forward CTGGCACCACCTTCTACA	This paper	N/A
Primer: mouse Actin-b gene Reverse TCATCTTTTACGGTTGGCTT	This paper	N/A
Software and algorithms		
R version 4.2.1	R Project	https://www.R-project.org/

RESOURCE AVAILABILITY

Lead contact

Further information and requests for resources and reagents should be directed to and will be fulfilled by the lead contact Rafael Sanjuán (rafael.sanjuan@uv.es).

Materials availability

All the unique reagents (resistant clones and viral constructs) developed in this work are available upon request.

Data and code availability

- Raw RNA-seq data were deposited at SRA and are publicly available as of the date of publication. Accession numbers are listed in the [key resources table](#).
- This paper does not report original code.
- Any additional information required to reanalyse the data reported in this paper is available from the [lead contact](#) upon request.

METHOD DETAILS

Virus strains

VSV wildtype (WT-mCherry) and oncolytic VSV (D51-GFP) were kindly provided by Dr. Valery Z. Grdzlishvili (University of North Carolina, USA). Both WT and D51 VSVs belong to the Indiana serotype. GFP and mCherry reporter genes were cloned at the intergenic region between the G and L genes. Sindbis virus (SBV-GFP), derived from plasmid infectious cDNA clone pTE/3'2J was kindly provided by Dr. Carla Saleh.

Cell lines and culture

B16-F10 (CVCL_1915), CT26 (CVCL-7255), and BHK-21 (CVCL_0159) cells were obtained from the American Type Culture Collection (ATCC) and cultured in DMEM supplemented with 10% fetal bovine serum (FBS), 1% non-essential amino acids, 50 U/mL penicillin and 50 µg/mL streptomycin. No information about the gender or exact age of the source animals was available. All cell lines were cultured at 37°C under 95% humidity, 5% CO₂, and regularly shown to be free of mycoplasma contamination by PCR.

Viral titration by plaque assay

Confluent BHK-21 monolayers were inoculated with 100 µL containing serial dilutions of the virus for 45 min and then overlaid with DMEM supplemented with 2% FBS and 0.5% agar. At 20–24 hours post inoculation

(hpi), cells were fixed with 10% formaldehyde and stained with 2% crystal violet in 10% formaldehyde to visualize plaques. Virus titers were calculated as plaque forming units (PFU) per mL.

Automated real-time fluorescence microscopy

Real-time live-cell fluorescence imaging was performed using an IncuCyte S3 Live-Cell Analysis System (Sartorius) placed inside a cell culture incubator. Images were acquired using phase contrast, green (300-ms exposure) and red (400-ms exposure) channels with a 4X objective. Representative images of various time points and experimental conditions were used as a reference to calibrate image analysis masks for each acquisition channel. Images were segmented by defining a fluorescence intensity threshold after applying a Top-Hat background correction.

Cell sorting and clonal expansion

Cells were detached using trypsin-EDTA, resuspended in DMEM containing 10% FBS, washed twice with PBS 1X by centrifugation (1200 rfc, 5 min), and finally resuspended in 1 mL of PBS containing 2% FBS at a cell concentration of 10^6 cells/mL. Approximately 10^6 events were analysed and naïve B16 and CT26 populations were used to delineate quadrants manually selecting survival, GFP-negative B16/CT26 cells. Selected cells were separated using a Beckman Coulter “MoFlo Legacy” cell sorter in 96-well plates and surviving cells were amplified by serial transfer to 48-well, 24-well, 60 mm, and 100 mm plates, and finally stored at -150°C .

RNA extraction, cDNA synthesis and quantitative PCR

RNA from 6-well confluent monolayers plates was extracted with RNAzol RT (Sigma-Aldrich) following manufacturer’s instructions and quantified by Nanodrop (Thermo Scientific). Approximately 1 μg of total RNA was subjected to reverse transcription using NZY reverse transcriptase (NZYtech) and specific plus-strand primers for VSV genes L (5' AACGATTCCCCACAAGATCCC) or P (5' CGCCAGAGGGTTTAAGTGGAG). Primers for cellular mRNAs included mouse *Mx2* (5' TGGAGTCGGATTGACATCTCTG), *Oasl* (5' TGATG GTGTCGCAGTCTTTGA), *Irf7* (5' GAGCCCAGCATTTTCTCTTG) and β -actin (5' CAGAGGCATACAGGGA CAGC). Reverse transcription (RT) reactions were performed at 50°C , following manufacturer’s instructions. Quantitative PCR (qPCR) was performed using primers for VSV gene L (5' AACGATTCCCCACAAGATCCC, 5' GCAAGAGGGTGGTGGAAATAGAG), VSV gene P (5' CGCCAGAGGGTTTAAGTGGAG, 5' TTCTGAT TGGGACGGATGTGTG), *Mx2* (5' ACACGGTCACTGAAATTGTACG, 5' TGGAGTCGGATTGACATCT CTG), *Irf7* (5' CCAGTTGATCCGCATAAGGT, 5' GAGCCCAGCATTTTCTCTTG), *Oasl* (5' TTGTGCGGAG GATCAGGTA, 5' TGATGGTGTGCGAGTCTTTGA) or β -actin (5'CTGGCACCACACCTTCTACA, 5'TCATCTTTTACGGTTGGCTT) using PowerUP SYBR Green qPCR Master Mix (Applied Biosystems) in a Quant Studio 3.0 qPCR thermocycler (Applied Biosystems). The following thermal profile was used for amplification: 95°C for 10 min, and 40 cycles of 95°C for 5 s, 55°C 10 min and 60°C for 20 s. The absence of primer dimers, contaminating cDNA in the mastermixes and multiple amplifications in the reactions were tested by melting curve analysis and by including no-RT and no-template controls.

Preparation of conditioned media

Confluent cell monolayers were inoculated with VSV-D51 at a multiplicity of infection (MOI) of 0.1 PFU/cell, supernatants were collected at 24 hpi, centrifuged at 1200 rfc for 10 min and passed through 0.05 μm cellulose filters (MF-Millipore) to remove viral particles. The undiluted medium was tested by the plaque assay to verify the absence of infectious particles, and this conditioned medium was aliquoted and stored at -80°C .

RNA extraction, quantitation, and integrity analysis for RNA sequencing

Each cell clone was seeded in triplicate and collected with RNAzol RT. The extraction was performed following manufacturer’s instructions as indicated above. Samples were quantified and checked for A260/280 and A260/230 quality ratios (>1.9). In-depth integrity quality analysis was performed in house using Agilent 2100 Bioanalyzer and externally (Novogene, Cambridge, UK).

cDNA library preparation and Illumina RNA sequencing

Poly-T oligo-attached magnetic beads were used for mRNA enrichment and purification from total RNA. After fragmentation, first-strand cDNA was synthesized using random hexamer primers, followed by second strand cDNA synthesis using dTTP for non-directional library. Libraries were quantified by absorbance

(Qubit) and qPCR, and size distribution was analysed (Bioanalyzer 2100). Library preparations were sequenced using the Illumina NovaSeq 6000 platform, which generated approximately 150 base paired-end raw reads. Raw sequences were deposited in the NCBI Short Read Archive (SRA) database under the BioProject accession numbers SRA: PRJNA824679, PRJNA855353 for B16 and CT26 respectively. Raw reads in FASTQ format were first processed using fastp. Clean reads were obtained by removing adapters, poly-N sequences and low-quality reads.

Gene expression quantitation and differential expression analysis

Reads were mapped to the *Mus musculus* genome using HISAT2 (v2.0.5). Featurecounts (v 1.5.0-p3) were used to obtain read counts for each gene and fragment per kilobase per million mapped reads (FPKM) were calculated. Differential expression analyses (three biological replicates per condition) were carried out to compare each VSV-resistant B16 or CT26 clone with treatment-naïve B16 or CT26 cells respectively using the DESeq2 (v1.20.0) R package, and the resulting P-values were adjusted using the Benjamini and Hochberg's approach to control for false discovery rate. Genes with an adjusted $p < 0.05$ were assigned as differentially expressed. Principal component analyses (PCA) were performed in R using variance-stabilizing-transformation (VST) normalisation of read counts. Hierarchical heatmap and cluster analysis were performed using coolmap (package limma) and hclust functions in R, based on relative gene distance.

Enrichment analyses

Gene Ontology (GO) enrichment analyses of differentially expressed genes were implemented using the ClusterProfiler (v3.8.1) R package, which corrects for gene length bias. GO terms with adjusted P-values lower than 0.05 were considered as significantly enriched. The observed gene ratio was defined as the fraction of all differentially expressed genes that belonged to a given GO term. The expected gene ratio was defined as the fraction of all genes in the GO database that belonged to a given GO term.

STRING protein-protein interaction analysis

The Search Tool for Retrieval of Interacting Genes and Proteins (STRING) database (<http://stringdb.org>) was used in order to construct protein-protein interaction networks. A sub selection of the two major gene clusters obtained by hierarchical clustering of the most differentially expressed genes between resistant and naïve B16 cells was used as network input. Known and predicted associations were scored and integrated (neighbourhood, gene fusion, co-occurrence, co-expression, experimental evidence, database evidence, evidence from text mining and homology between two proteins).

Immunofluorescence and confocal microscopy images

Treatment-naïve and resistant B16 cells were seeded in triplicate in 24-well plates containing circular coverslips and allowed to grow to confluence. Cells were fixed with 3.6% PFA for 30 min at 4°C, washed twice with 1X PBS, and incubated in blocking solution (20% goat serum, 0.5% Triton X-100 in 1X PBS) for 2 h with shaking at room temperature. Endogenous immunoglobulin blocking was performed with AffiniPure Fab Fragment Goat Anti-Mouse IgG (Jackson ImmunoResearch) diluted in blocking solution and incubated for 2 h at 4°C. Cells were washed with PBS and then incubated with Mx1/2/3 mouse monoclonal primary antibody (1:500, Santacruz Biotech) overnight at 4°C. After primary incubation, cells were washed twice with 1X PBS and incubated with Alexa Fluor Plus 594 Mouse IgG (H + L) polyclonal secondary antibody (1:1000, Invitrogen), 1 h at room temperature and mounted with ProLong Gold antifade reagent containing DAPI (Invitrogen) on separate slides. Samples were imaged on a FV1000 confocal microscope (Olympus). Cell auto fluorescence and non-specific secondary antibody binding were tested using no secondary antibody and no primary antibody controls.

QUANTIFICATION AND STATISTICAL DETAILS

All infections were conducted in triplicates and all measurements are reported as mean \pm SEM. Statistical analyses were performed using SPSS software (IBM Analytics). Mapping, read counts, differential gene expression, Gene Ontology and KEGG analysis were carried out in R (4.2.1), packages as indicated in [methods details](#). For all statistical tests, a p value of 0.05 was accepted for statistical significance; additional details in figure legends.